

Acoustic radiation torque of an acoustic-vortex spanner exerted on axisymmetric objects

Yuzhi Li, Gepu Guo, Juan Tu, Qingyu Ma, Xiasheng Guo, Dong Zhang, and Oleg A. Sapozhnikov

Citation: *Appl. Phys. Lett.* **112**, 254101 (2018); doi: 10.1063/1.5036976

View online: <https://doi.org/10.1063/1.5036976>

View Table of Contents: <http://aip.scitation.org/toc/apl/112/25>

Published by the [American Institute of Physics](#)

AIP | Conference Proceedings

Get **30% off** all
print proceedings!

Enter Promotion Code **PDF30** at checkout



Acoustic radiation torque of an acoustic-vortex spanner exerted on axisymmetric objects

Yuzhi Li,¹ Gepu Guo,¹ Juan Tu,² Qingyu Ma,^{1,2,a)} Xiasheng Guo,² Dong Zhang,^{2,a)} and Oleg A. Sapozhnikov^{3,4}

¹Key Laboratory of Optoelectronics of Jiangsu Province, School of Physics and Technology, Nanjing Normal University, Nanjing 210023, China

²Institute of Acoustics, Nanjing University, Nanjing 210093, China

³Center for Industrial and Medical Ultrasound, University of Washington, Seattle, Washington 98105, USA

⁴Department of Acoustics, Physics Faculty, Moscow State University, Moscow 119991, Russia

(Received 19 April 2018; accepted 30 May 2018; published online 19 June 2018)

Based on the analysis of the wave vector of an acoustic-vortex (AV) spanner, the radiation torque of object rotation is investigated. It is demonstrated that the rotation of an axisymmetric disk centered on the AV spanner is mainly driven by the acoustic radiation force. The radiation torque exerted on a small-radius object is inversely associated with the topological charge in the center AV, and it is enhanced significantly for a larger AV with a higher topological charge. With the sixteen-source experimental setup, radius dependencies of radiation torque for AV spanners with different topological charges are verified by quantitative laser-displacement measurements using disks with different radii. The favorable results demonstrate that the radiation torque is more applicable than the orbital angular momentum in describing the driving capability of an AV spanner and can be used as an effective tool in clinical applications to manipulate objects with a feature size at the wavelength-scale inside body. *Published by AIP Publishing.* <https://doi.org/10.1063/1.5036976>

Based on the concept of optical vortices,^{1–8} the acoustic vortex (AV) was proposed to have helical wavefronts with indeterminate phases and pressure nulls along the propagation axis,^{9–17} possessing the capability of particle manipulation with the acoustic radiation force (ARF) and the orbital angular momentum (OAM). The circular phase variation around the core can be described by the topological charge l ,¹⁸ indicating how many phase twists the acoustic wave undergoes in one circle. Small objects can be driven to rotate around the center axis along the acoustic beam and show potential applications in object alignment and particle manipulation.^{19,20} Compared with optical vortices, the AV beam can be formed in deep tissues, thus exhibiting the application potential in non-invasive treatment and targeted drug delivery²¹ in biomedical engineering.

In the past few decades, the study of AVs has attracted more and more attention in the discussion of acoustic tweezers and acoustic spanners. Based on the solution of the Helmholtz equation, the intrinsic properties of AVs were explained by Lekner²² and the corresponding OAM was calculated *via* quantum mechanics. Zhang²³ concluded that the radiation torque exerted on an axisymmetric object centered on the beam axis could be calculated as the integral of the time-averaged flux of the OAM density over the total field, which was proportional to the power absorbed by the object with a factor of l/ω at the angular frequency ω . An interpretation of the AV in free space was proposed by Volke-

Sepúlveda,²⁴ and the difference was evaluated for AVs with $l=1$ and 2. A torsion pendulum¹⁹ was used to measure the OAM transferred to hanging disks of several sizes using a four-source array. A quantitative test of the OAM transferred to an acoustic absorbing object was performed by Anhauser²⁵ using the torque balance in a viscous liquid. A phase-coded approach²⁶ was proposed to generate an AV beam with controllable l with a maximal value determined by the source number.

In the previous studies done by Lekner and Volke-Sepúlveda,^{22,24} the capability of object rotation was reported to be produced by the transferred OAM $L_z = \rho(\mathbf{r} \times \mathbf{v}_\perp) = \pm(\rho l \varepsilon)/\omega$, where \mathbf{v}_\perp is the transverse particle velocity, ρ is the density of the medium, and ε is the energy density. It was obvious that faster object rotation could be produced by a greater OAM of the AV with a higher l . However, Volke-Sepúlveda²⁴ observed that the radiation torque for $l=2$ was smaller than that for $l=1$ for a small suspension disk. In an ideal medium without viscosity and dissipation, the particle velocity can be calculated by $\mathbf{v} = -\nabla p/(i\omega\rho)$. Although \mathbf{v} is irrotational, the ARF exerted on the object is the time-average of the acoustic pressure along the normal direction of the wavefront.^{27–29} Thus, the ARF and the corresponding radiation torque of an AV spanner can be used properly to investigate the property of object rotation instead of the OAM.

In this letter, theoretical and numerical studies on the ARF based radiation torque of an AV spanner generated by a circular array of point sources were conducted based on the analysis of wave vector. A laser-displacement indicator device was established to measure the radiation torque quantitatively using a sixteen-source AV system. Consistent results between numerical simulations and experimental

^{a)}Authors to whom correspondence should be addressed: maqingyu@nju.edu.cn and dzhang@nju.edu.cn. Telephone: 86-25-85891905, Mobile: 86-13770847142. Present address: School of Physics and Technology, Nanjing Normal University, 1 Wenyuan Road, Xianlin District, Nanjing 210023, China.

measurements indicated that the radiation torque was determined by the radius of the object and the topological charge of the AV spanner. The radiation torque was inversely associated with l for a small-radius object, and it was enhanced significantly for a larger AV with a higher l . The special case²³ of the radiation torque proportional to l could not be realized in the observation range. The favorable results suggested that the radiation torque was more applicable than the OAM in describing the driving capability of object rotation and might be used in biomedical areas as an effective method to manipulate objects with a wavelength-scale featured size (e.g., kidney stone in lithotripsy).

The phase-coded approach²⁶ is applied to a circular source array according to the schematic diagram as shown in Fig. 1. N acoustic sources are positioned on a circumference (radius a) with a spatial angle difference $\Delta\varphi = 2\pi/N$. In cylindrical coordinates, the position of the n th source can be described as $(a, \varphi_n, 0)$ with $\varphi_n = 2\pi(n-1)/N$. When the sources are excited by N sinusoidal waveforms with a phase difference $\Delta\phi = l\Delta\varphi$, the acoustic pressure at (r, φ, z) produced by the n th source can be written as

$$p_n(r, \varphi, z, t) = (A_0/R_n)\exp(i\omega t)\exp(-ikR_n)\exp(\pm i\phi_n), \quad (1)$$

where A_0 is the source pressure, $k = \omega/c$ is the wave number for the acoustic speed c , R_n is the propagation distance from $(a, \varphi_n, 0)$ to (r, φ, z) , and t is the transmission time. Thus, the total acoustic pressure at (r, φ, z) can be calculated by

$$p(r, \varphi, z, t) = \sum_{n=1}^N (A_0/R_n)\exp(i\omega t)\exp(-ikR_n)\exp(\pm i\phi_n). \quad (2)$$

$p(r, \varphi, z, t)$ is a plural, comprising the phase of the helical wavefront by $\Phi(r, \varphi, z, t) = \arctan[\text{Im}(p)/\text{Re}(p)]$. By taking $\nabla\Phi = (\partial\Phi/\partial x, \partial\Phi/\partial y, \partial\Phi/\partial z)$, the direction of the ARF can be achieved by the normal direction of the wavefront.

The ARF in an acoustic field can be calculated by $d\mathbf{F} = \langle \rho\mathbf{v}(\mathbf{v} \cdot \mathbf{n}) + \left(\frac{\rho\langle p^2 \rangle}{2\rho c^2} - \frac{\rho\langle \mathbf{v} \cdot \mathbf{v} \rangle}{2}\right) \mathbf{n} \rangle dS$,^{27,28} where $\langle \cdot \rangle$ is the time-averaged calculation over the period $2\pi/\omega$ and \mathbf{n} is the unit vector of the ARF perpendicular to the surface element dS . The term $\rho\mathbf{v}(\mathbf{v} \cdot \mathbf{n})$, known as Reynold's stress,^{27,30} originates from the momentum equation and is produced by

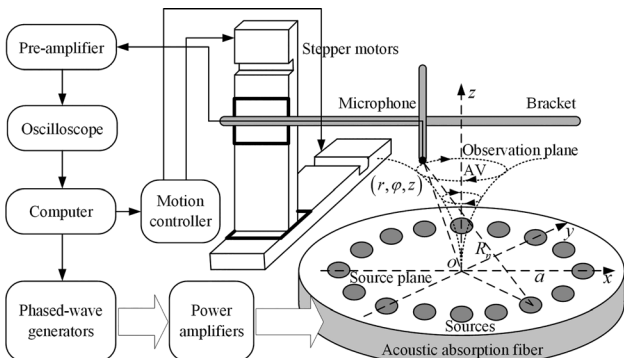


FIG. 1. Schematic diagram of the AV generation and scanning measurement system.

changing from the Eulerian to the Lagrangian reference frame due to the motion of the fluid particle at the boundary, which is negligible for small amplitude acoustic vibrations. Therefore, the radiation torque in an AV spanner can be calculated by $\mathbf{M} = \iint_S \mathbf{r} \times d\mathbf{F}$, where $d\mathbf{F} = \left(\frac{\langle p^2 \rangle}{2\rho c^2} - \frac{\rho\langle \mathbf{v} \cdot \mathbf{v} \rangle}{2}\right) \mathbf{n} dS$ represents the ARF exerted on dS . Since the component along the z direction of the ARF does not contribute to disk rotation, \mathbf{n} can be replaced by its transverse projection $\mathbf{n}_\perp = \left(\frac{\partial\Phi}{\partial x}, \frac{\partial\Phi}{\partial y}\right) / \left|\left(\frac{\partial\Phi}{\partial x}, \frac{\partial\Phi}{\partial y}\right)\right|$ and the radiation torque can be achieved by

$$\mathbf{M} = \iint_S \mathbf{r} \times \left(\frac{\langle p^2 \rangle}{2\rho c^2} - \frac{\rho\langle \mathbf{v} \cdot \mathbf{v} \rangle}{2}\right) \mathbf{n}_\perp dS. \quad (3)$$

It shows that besides the acoustic pressure, the radiation torque of an AV spanner is also influenced by the angle between the normal direction of the wavefront and the transverse plane. For a fixed transducer array, the radiation torque of the AV spanner is influenced by the structure of the topological-charge determined helical wavefronts.

Numerical studies were conducted for $N=16$, $a=30$ cm, and $f=1.3$ kHz in air with $c=342$ m/s and $\Delta\varphi = 2\pi l/16$ for $l=1$ to 7. Axial pressure profiles (line 1) and cross-sectional distributions of pressure (line 2) and phase (line 3) for AVs with $l=1$ to 4 (column 1 to 4) at $z=15$ cm are presented in Fig. 2. The presence of the AV spanner is proved by the concentric pressure circles with an obvious phase spiral and center pressure null. As shown in Fig. 2(1- l), for each l , the radius of the AV at the source plane is the smallest, and an expanded AV spanner can be generated at a longer z with a decreased peak pressure (P_p). At a fixed z , a bigger radius with more divergent energy is generated for a higher l . With the increase in l , the radii of the pressure peak (R_{pp}) and pressure valley (P_v, R_{pv}) increase accordingly with an expanded vortex center. Corresponding to Fig. 2(2- l), an anti-clockwise phase spiral is displayed in Fig. 2(3- l) with a phase variation of $2\pi l$. Moreover, compared to the center AV in $r < R_{pp}$, the contribution of the surrounding AV on object rotation is relatively low due to the weaker

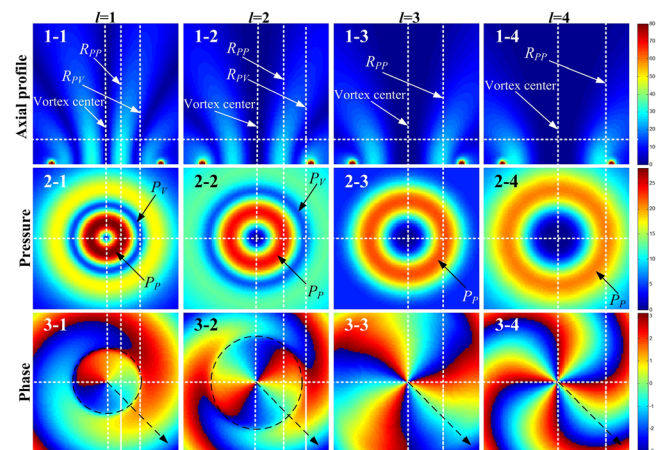


FIG. 2. Axial profiles (line 1) and cross-sectional distributions of pressure (line 2) and phase (line 3) for AV spanners with the topological charges of 1, 2, 3, and 4 at $z=15$ cm.

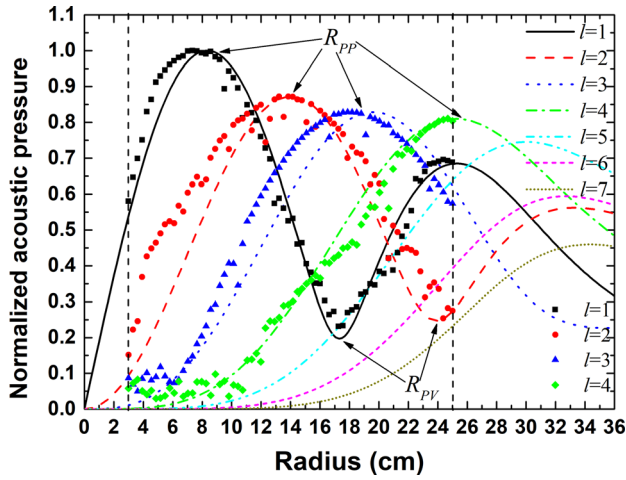


FIG. 3. Normalized radial pressure distributions of AV spanners with different topological charges at $z = 15$ cm.

tangential component of the ARF. Therefore, as indicated by the phase circles in Figs. 2(3-1) and 2(3-2), R_{PV} can be treated as the effective radius of an AV spanner. Based on the radial pressure distributions as shown in Fig. 3, one can find that, with the increase in r , the acoustic pressure increases from $r = 0$ to P_P at R_{PP} and then goes down to P_V at R_{PV} . For $l = 1$ to 7, R_{PP} increases monotonically from 8.4 to 34.0 cm with a decreased P_P from 1 to 0.46. Due to the influence of sources, only two P_V s at $R_{PV} = 17.4$ and 24.0 cm are formed for $l = 1$ and 2, whereas for $l > 3$, the acoustic pressure drops monotonically from its P_P without the generation of P_V in the observation range.

A disk centered on the AV was assumed to hang horizontally at $z = 15$ cm to calculate the radiation torque. The radiation torque distributions for $l = 1$ to 7 as plotted in Fig. 4 show an increasing tendency with respect to r . In $r < 15.3$ cm, a radiation torque sequence (S_M) is obtained as $S_M(1, 2, 3, 4, 5, 6, 7)$, indicating that the radiation torque is inversely associated with l . Due to the decline of the acoustic pressure after P_P , the growth rates of radiation torque decrease gradually for $l = 1$ and 2, until reaching zero at $R_{PV} = 17.4$ and 24 cm. Meanwhile, rapid growths of radiation torque for $l > 2$ are observed because of the continuous

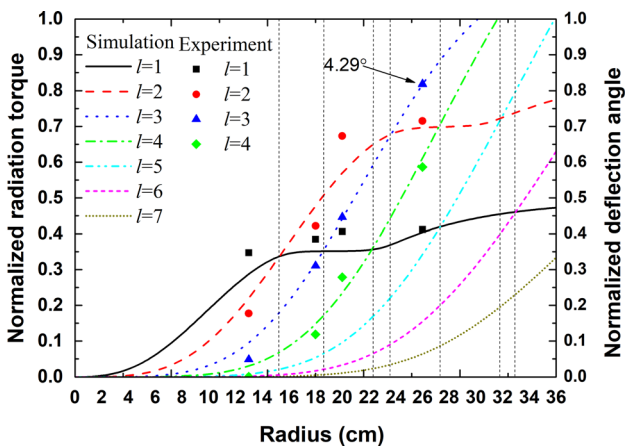


FIG. 4. Radius dependencies of radiation torque for AV spanners with different topological charges at $z = 15$ cm with the corresponding deflection angles measured for disks with various radii.

increase in the acoustic pressure. When $r = 15.3, 18.5, 22.3, 23.6,$ and 27.3 cm, the radiation torque sequences are $S_M(2, 1, 3, 4, 5, 6, 7)$, $S_M(2, 3, 1, 4, 5, 6, 7)$, $S_M(2, 3, 4, 1, 5, 6, 7)$, $S_M(3, 2, 4, 1, 5, 6, 7)$, and $S_M(3, 4, 2, 5, 1, 6, 7)$, respectively. The special sequence $S_M(7, 6, 5, 4, 3, 2, 1)$ ²²⁻²⁴ does not appear in the observation range, which might be realized when the disk radius is much larger than the wavelength, which is consistent with the conclusion claimed by Zhang and Marston.²³ Therefore, for a small disk with the radius less than half wavelength, a larger radiation torque can be generated by an AV spanner with a smaller l . With the increase in r , an enhanced radiation torque can be produced by the expanded AV with a larger l .

An experimental system, as illustrated in Fig. 1, was established with the parameters consistent with those used in simulations. Sixteen speakers (diameter: 8 cm; power: 10 W) with cylindrical waveguides (radius: 1 cm) were distributed on a circumference ($a = 30$ cm). Sixteen sinusoidal signals with controllable phases²⁶ were sent out and then amplified to drive the speakers to emit acoustic beams. The topological charge was adjusted by the phase difference $l\pi/8$ for $l = -7$ to 7. With the stepper motor (Newport M-ILS250, Newport Corporation, USA) controlled by the motion controller (Newport ESP301, Newport Corporation, USA), radial pressure distributions were measured using a mini-microphone (diameter 4 mm, Panasonic WM-61B102C, Japan) (Newport M-ILS250, Newport Corporation, USA) and collected using a digital oscilloscope (Agilent DSO9064A, Agilent Corporation, USA).

As illustrated in Fig. 5, a laser-displacement (angle) measurement system was developed to measure the radiation torque of the AV spanner. Under a coaxially hanging circular acrylic disk, a sponge layer with a 2-cm thickness was adhered to absorb acoustic waves from below. A soft cotton thread was connected to the center of the disk to provide weight support, and an elastic rubber hose with a fixed length was applied to measure the radiation torque. A laser beam emitted by a laser diode fixed at the center of the disk was used to indicate its deflection angle by the displacement, which was measured at 5-m away from the disk center. Driven by the AV spanner, an opposite resistance torque could be generated by the twisted rubber hose. When it reached torque balance, the radiation torque exerted on the disk could be evaluated by the approximate linear relation

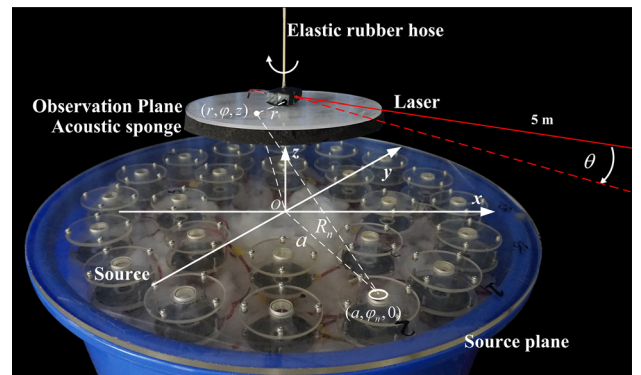


FIG. 5. Sketch map of radiation torque measurement for AV spanners with a laser-displacement (angle) indicator.

$M = -\kappa\theta$, where κ was the rotational stiffness of the rubber hose and θ was the deflection angle.

Due to the range limit of the stepper motor, radial pressure distributions were measured from 3 to 25 cm at the step of 0.3 mm for $l = 1$ to 4, which are plotted in Fig. 2. The experimental results are in good agreement with the simulations, especially for the similar locations and amplitudes of P_p and P_v . For each l , the acoustic pressure in the center region of the AV spanner is relatively low and it increases accordingly with an increased r until reaching its P_p . In addition, for $l = 1$ to 4, the deflection angles were measured for four disks with the radii of 13, 18, 20, and 26 cm. As plotted in Fig. 4, the experimental results of the measured radiation torque were normalized by the maximum displacement of 37.5 cm (deflection angle 4.29°) for $r = 26$ cm and $l = 3$. The consistent radiation torque sequences of $S_M(1, 2, 3, 4)$, $S_M(2, 1, 3, 4)$, $S_M(2, 3, 1, 4)$, and $S_M(3, 2, 4, 1)$ demonstrate the feasibility of the accurate radiation torque measurement for an AV spanner using disk deflection.

Because of the emphasis on optical vortices in previous studies, the OAM transfer is often used to describe the characteristics of AVs. However, in practical applications, it is impossible to measure the OAM at one point inside an object accurately. Contrary to the OAM, the ARF with the direction of the wave vector \mathbf{k} is not affected by the irrotationality of the instantaneous vibration velocity, which can be used to analyze the object rotation for an AV spanner. Meanwhile, the OAM transferred to the object can also be achieved from the measured radiation torque with a known shape in the transverse plane, which is especially applicable for the object with a feature size at the wavelength-scale (e.g., kidney stone in lithotripsy).

In the field of acoustofluidics,³¹ acoustic streaming has emerged as a promising technology for refined microscale manipulation with a strong rotational flow of the microvortex, which is rapidly tunable and highly scalable. With a continuous narrow-beam focused surface wave at a frequency of 381 MHz, acoustic streaming vortices were generated to selectively capture particles and cells with different radii.³² Tang *et al.* showed that, by an ultrasonically vibrating needle inserted in a droplet, the spiral vortex of acoustic streaming could be generated to concentrate SiO₂ particles with the initial concentration of 0.09 mg/ml to the spot with the diameter of several hundred microns.³³ It had also been reported that, by using two orthogonal standing waves with a phase lag, microfluidic vortices could be generated between an elastic solid wall and a rigid reflector.³⁴ The feasibility of rotating and moving fluid particles using the vortices was also demonstrated. Regardless of different generation mechanisms, the vortices generated by the acoustic streaming and the AV spanner can both be used to trap and manipulate micro particles using the OAM or ARF. Further investigations on the integrated system using the two kinds of vortices might enable more opportunities for the application of particle manipulation technology in the biomedical area.

Although the radius dependencies of radiation torque for AVs with different l are studied qualitatively, some discrepancies can still be observed between theoretical and experimental results. One potential error is that, because the size of experimental sources is not much smaller than the

wavelength, the simplified assumption of the point source is not completely accurate. Further, the perfect generation of an AV spanner cannot be realized because of the uncertain factors of the pressure consistency and the phase accuracy of sources. In addition, the experimental measurements are also influenced by the inhomogeneity of materials, such as the roughness of the sponge, the nonlinear elasticity of the rubber hose, the acoustic reflection of the bracket, and so on.

In conclusion, with the analyses of the wavefront and wave vector for AV spanners generated by the phased-coded approach using a circular transducer array, the radius dependencies of radiation torque for AV spanners with different l are investigated for objects with various sizes. It is proved that a more concentrated AV spanner with a smaller radius and a higher peak pressure can be generated by a smaller l . The rotation of the axisymmetric disk centered on the AV spanner is driven by the exerted radiation torque, which is inversely associated with l for a small-radius object. For larger objects, a higher l should be selected to enhance the radiation torque of the bigger AV. With the laser-displacement indicator, the theoretical results are verified by the measured radiation torques of AV spanners with different l for disks with various radii. The favorable results demonstrate that the radiation torque of an AV spanner is more applicable to understanding origin of object rotation, especially for the object with a feature size at the wavelength-scale (e.g., kidney stone in lithotripsy). Although only the low-frequency sound is employed in this study, the conclusions can be extended to the high-frequency ultrasound^{25,35,36} in water, which might enable more potential applications for non-invasive object manipulation inside body.

We would like to thank Professor Thomas J. Matula (University of Washington, USA), Professor Jianchun Cheng (Nanjing University, China), and Dr. Likun Zhang (University of Texas at Austin, USA) for their assistance in this research. This work was supported by the National Natural Science Foundation of China (Grant Nos. 11474166 and 11604156), the Natural Science Foundation of Jiangsu Province (No. BK20161013), the Postdoctoral Science Foundation of China (No. 2016M591874), the Postgraduate Research and Practice Innovation Program of Jiangsu Province (KYCX17_1083), and the Priority Academic Program Development of Jiangsu Higher Education Institutions, China.

¹M. V. Berry and S. Klein, *J. Mod. Opt.* **43**, 165 (1996).

²N. B. Simpson, *Opt. Lett.* **22**, 52 (1997).

³M. V. Berry and S. Popescu, *J. Phys. A: Math. Gen.* **39**, 6965 (2006).

⁴G. Mariyenko, J. Strohaber, and C. J. G. J. Uiterwaal, *Opt. Express* **13**, 7599 (2005).

⁵P. Z. Dashti, F. Alhassen, and H. P. Lee, *Phys. Rev. Lett.* **96**, 043604 (2006).

⁶J. Courtial and K. O'Holleran, *Eur. Phys. J. Spec. Top.* **145**, 35 (2007).

⁷N. Yu and Z. Gaburro, *Science* **334**, 333 (2011).

⁸J. Xavie, R. Dasgupta, S. Ahlawat, J. Joseph, and P. Kumar Gupta, *Appl. Phys. Lett.* **100**, 121101 (2012).

⁹J. F. Nye and M. V. Berry, *Proc. R. Soc. London, Ser. A* **336**, 165 (1974).

¹⁰J. L. Thomas and R. Marchiano, *Phys. Rev. Lett.* **91**, 244302 (2003).

¹¹K. Y. Bliokh and V. D. Freilikher, *Phys. Rev. B* **74**, 174302 (2006).

¹²J. Lekner, *Phys. Rev. E* **75**, 036610 (2007).

- ¹³R. Marchiano, F. Coulouvrat, L. Ganjehi, and J. L. Thomas, *Phys. Rev. E* **77**, 016605 (2008).
- ¹⁴R. Marchiano and J. L. Thomas, *Phys. Rev. E* **71**, 066616 (2005).
- ¹⁵B. Aronov, D. A. Brown, C. L. Bachand, and X. Yan, *J. Acoust. Soc. Am.* **131**, 2079 (2012).
- ¹⁶O. Santillán and K. Volke-Sepúlveda, *Am. J. Phys.* **77**, 209 (2009).
- ¹⁷A. Cain and S. Umemura, *IEEE Trans. Microwave Theory Tech.* **34**, 542 (1986).
- ¹⁸M. Berry, *Nature* **403**, 21 (2000).
- ¹⁹K. D. Skeldon, C. Wilson, M. Edgar, and M. J. Padgett, *New J. Phys.* **10**, 013018 (2008).
- ²⁰S. T. Kang and C. K. Yeh, *IEEE Trans. Ultrason. Ferroelectr. Freq. Control* **57**, 1451 (2010).
- ²¹T. Brunet, J. L. Thomas, and R. Marchiano, *Phys. Rev. Lett.* **105**, 034301 (2010).
- ²²J. Lekner, *J. Acoust. Soc. Am.* **120**, 3475 (2006).
- ²³L. Zhang and P. L. Marston, *Phys. Rev. E* **84**, 065601 (2011).
- ²⁴K. Volke-Sepúlveda, A. O. Santillán, and R. R. Boullosa, *Phys. Rev. Lett.* **100**, 024302 (2008).
- ²⁵A. Anhauser, R. Wunenburger, and E. Brasselet, *Phys. Rev. Lett.* **109**, 034301 (2012).
- ²⁶L. Yang, Q. Ma, J. Tu, and D. Zhang, *J. Appl. Phys.* **113**, 154904 (2013).
- ²⁷C. P. Lee and T. G. Wang, *J. Acoust. Soc. Am.* **94**, 1099 (1993).
- ²⁸J. C. Cheng, *Principles of Acoustics* (Science Express, Beijing, 2012).
- ²⁹G. T. Silva, S. Chen, J. F. Greenleaf, and M. Fatemi, *Phys. Rev. E* **71**, 056617 (2005).
- ³⁰F. G. Mitri, *New J. Phys.* **8**, 138 (2006).
- ³¹D. J. Collins, B. Morahan, J. Garcia-Bustos, C. Doerig, M. Plebanski, and A. Neild, *Nat. Commun.* **6**, 8686 (2015).
- ³²D. J. Collins, B. L. Khoo, Z. Ma, A. Winkler, R. Weser, H. Schmidt, J. Han, and Y. Ai, *Lab Chip* **17**, 1769 (2017).
- ³³Q. Tang, X. Wang, and J. Hu, *Appl. Phys. Lett.* **110**, 104105 (2017).
- ³⁴A. A. Doinikov, P. Thibault, and P. Marmottant, *Ultrasonics* **87**, 7 (2018).
- ³⁵Y. Li, G. Guo, Q. Ma, J. Tu, and D. Zhang, *J. Appl. Phys.* **121**, 164901 (2017).
- ³⁶Q. Wang, Y. Li, Q. Ma, G. Guo, J. Tu, and D. Zhang, *J. Appl. Phys.* **123**, 034901 (2018).